RESEARCH ARTICLE

Mathematical Modeling of Rabies Control: Evaluating Vaccination Strategies via NSFD and RK4 Approaches

Hazrat Younas[1], **Imtiaz Ahmad**[1,*], **Zakir Ullah**[1] **and Hanif Ullah**[1]

[1] Department of Mathematics, University of Malakand, Chakdara 18000, Pakistan

Abstract

The initial mathematical model for rabies consists of six compartments representing the human and dog populations: $S_h, I_h, V_h, S_d, I_d, V_d$. To obtain a more realistic description of rabies transmission dynamics, we extend the model by introducing two additional human compartments: Exposed (E_h) and Recovered (R_h) individuals. The extended system therefore comprises eight compartments: $S_h, E_h, I_h, V_h, R_h, S_d, I_d, V_d$. This extension captures important differences in disease progression, treatment response, and transmission pathways. Within this framework, we examine the positivity and boundedness of solutions, derive the basic reproduction number (R_0), analyse the sensitivity of R_0 to key epidemiological parameters, and investigate the global stability of the endemic equilibrium. Numerical simulations are carried out using both the classical fourth-order Runge-Kutta (RK4) method and the Nonstandard Finite Difference (NSFD) method, allowing us to compare their accuracy and reliability in predicting population dynamics.

Keywords: rabies, stability analysis, RK4 versus the NSFD method.

1 Introduction

Rabies is caused by a neurotropic virus belonging to the genus *Lyssavirus* and the family *Rhabdoviridae*. The term "lyssa" originates from the Greek word meaning “frenzy” or “rage,” reflecting the furious behavior often exhibited by infected animals [1]. The central nervous system (CNS) is the primary target of the rabies virus, eventually leading to progressive and irreversible encephalitis and death. Dogs are the major source of most human rabies cases worldwide. Rabies is an acute and fatal zoonotic viral disease that affects nearly all mammalian species [2, 3]. Animal saliva is the principal reservoir of the virus, although it may also be present in tears, urine, semen, and other bodily fluids [4]. Rabies has one of the highest case-fatality rates among viral diseases, approaching almost 100% [6]. Once clinical signs appear, the infection is invariably fatal [7]. Humans contract rabies primarily from dogs, and transmission most commonly occurs through bites or scratches from infected animals [8, 9]. Direct contact between a wound or mucosal surface (such as the mouth, nose, or eyes) and the saliva of a rabid dog can also transmit the virus [10]. Rabies may additionally spread through aerosol exposure or through tissue

Submitted: 30 January 2026
Accepted: 03 March 2026
Published: 15 April 2026

Vol. 2, **No.** 1, 2026.
10.62762/JNSPM.2026.413156

***Corresponding author:**
✉ Imtiaz Ahmad
mathskhan18@gmail.com

Citation
Younas, H., Ahmad, I., Ullah, Z., & Ullah, H. (2026). Mathematical Modeling of Rabies Control: Evaluating Vaccination Strategies via NSFD and RK4 Approaches. *Journal of Numerical Simulations in Physics and Mathematics*, 2(1), 9–24.

and organ transplantation in both humans and other species [11]. Early symptoms of rabies include fever, discomfort, tingling or unusual sensations at the bite site (paraesthesia), hypersalivation, sore throat, cough, nausea, and vomiting [12]. These symptoms resemble those of influenza. As the virus progresses to the CNS, the brain and spinal cord begin to swell progressively, leading to paralysis, hyperactivity, and ultimately death [13]. According to the World Health Organization (WHO), rabies is a 100% vaccine-preventable disease [14]. Three primary strategies for rabies control have been identified [15]: population management, mass dog vaccination, and epidemiological surveillance. Mathematical modeling has provided valuable insights into the mechanisms underlying complex biological systems and offers practical and optimal solutions for disease control, as demonstrated in real-world urban settings [5]. Motivated by these considerations, several mathematical models of rabies have been developed in recent years, including models incorporating vaccination and post-treatment effects [17]. Unlike many existing models, our study does not incorporate explicit time delays, focusing instead on the immediate dynamics of transmission. The model includes transmission from dogs to humans and among dogs themselves, resulting in a system of delay differential equations. Furthermore, we propose three control strategies annual puppy birth control and vaccination of both humans and dogs aimed at reducing the burden of rabies within human and canine populations. The main objectives are to investigate the effects of time delay and control strategies on the dynamical behavior of the model and to assess the persistence and endemicity of the rabies virus within the interacting populations.

2 Model formulation

Two populations are represented in the model dogs and people coexisting in the same space. Three sub-populations comprise the human population at any given moment t) susceptible humans $S_h(t)$, infected humans $I_h(t)$, and vaccinated humans $V_h(t)$. $R_h(t)$ represent the recovered population. Thus, $N_h(t)$, which represents the whole human population, may be stated as follows:

$$N_h(t) = S_h(t) + E_h(t) + I_h(t) + V_h(t) + R_h(t), \quad (1)$$

Similarly, at any given time t, the dog population is divided into three sub-populations: susceptible dogs $S_d(t)$, and $E_h(t)$ Exposed population, infected dogs $I_d(t)$, and vaccinated dogs $V_d(t)$. As a result, the whole dog population is represented by $N_d(t)$,

$$N_d(t) = S_d(t) + V_d(t) + I_d(t).$$

The equation of the proposed model is

$$\begin{cases} \frac{dS_h(t)}{dt} &= K_h + \alpha_3 V_h - (v + \mu_h + \beta_{hd} I_d) S_h, \\ \frac{dE_h(t)}{dt} &= \beta_{hd} S_h I_d - (\alpha_1 + \alpha_2 + \delta + \mu_h) E_h, \\ \frac{dI_h(t)}{dt} &= \delta E_h - (\mu_h + \mu_1) I_h, \\ \frac{dV_h(t)}{dt} &= \alpha_1 E_h + v S_h - (\alpha_3 + \mu_h) V_h, \\ \frac{dR_h(t)}{dt} &= \alpha_2 E_h - \mu_h R_h, \\ \frac{dS_d(t)}{dt} &= K_d + k_1 V_d - (k + \beta_{dd} I_d) S_d, \\ \frac{dV_d(t)}{dt} &= k S_d - (\mu_d + k_1) V_d, \\ \frac{dI_d(t)}{dt} &= \beta_{dd} S_d I_d - \mu_d I_d. \end{cases} \quad (2)$$

Initial conditions are $S_h(0) > 0$, $E_h(0) \geq 0$, $I_h(0) \geq 0$, $V_h(0) \geq 0$, $S_d(0) > 0$, $I_d(0) \geq 0$.

Figure 1 shows the proposed model.

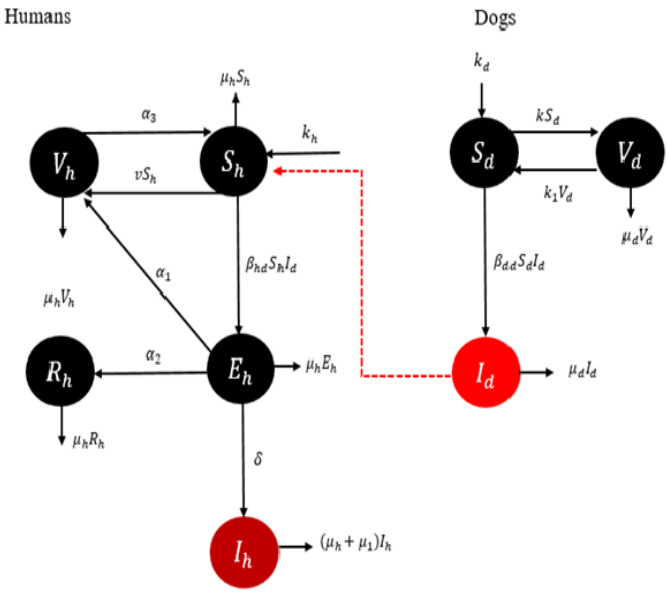

Figure 1. Flow chart of the proposed model

The parameters used in the model are summarized in Table 1.

All parameters are assumed to be non-negative, with $\mu_h, \mu_d > 0$ to ensure biological feasibility.

3 Model Analysis

We now examine the physiologically viable region of model system (1). Considering its two components,

Table 1. Model parameters and descriptions.

Parameter	Description	Dimension
K_h	Human birth/recruitment rate	persons/day
K_d	Dog birth/recruitment rate	dogs/day
α_1	Progression rate from exposed to infected (human)	1/day
α_2	Recovery rate from exposed (human)	1/day
α_3	Rate of losing vaccine-induced immunity (human)	1/day
μ_h	Natural death rate of humans	1/day
μ_d	Natural death rate of dogs	1/day
μ_1	Disease-induced death rate of humans	1/day
β_{hd}	Dog-to-human transmission rate	1/(dogs·day)
β_{dd}	Dog-to-dog transmission rate	1/(dogs·day)
δ	Progression rate from exposed to infected (human)	1/day
v	Human vaccination rate	1/day
k	Dog vaccination rate	1/day
k_1	Rate of losing vaccine-induced immunity (dogs)	1/day

the feasible region is defined as $\Omega = \Omega_h \times \Omega_d$ [10]. ***lemma:*** *The feasible area Ω still contains the solution set $\{S_h, E_h, I_h, V_h, R_h, S_d, I_d, V_d\} \in \mathbb{R}^8_+$ of the model system (1).*

Proof For any $t > 0$, $\{S_h, E_h, I_h, V_h, R_h, S_d, I_d, V_d\} \in R^8_+$, let's say we want to study the dynamics of model system (1) by demonstrating that the domain Ω is positively invariant.

$$N_h(t) = S_h(t) + E_h(t) + I_h(t) + V_h(t) + R_h(t), \quad (3)$$

$$N_d(t) = S_d(t) + I_d(t) + V_d(t), \quad (4)$$

where the total number of dogs at any one time is represented by $N_d(t)$. The total number of persons at any particular time is shown by N_h and (t). (t) Equation 5 gives

$$\frac{dN_h(t)}{dt} = K_h - \mu_1 I_h - \mu_h N_h \quad (5)$$

Similarly, equation

$$\frac{dN_d}{dt} = K_d - \mu_d N_d \quad (6)$$

Assuming that the dogs' compartment has no culling effects or disease-related mortality rates, 5 and 6 now become,

$$\frac{N_h(t)}{dt} = K_h - \mu_h N, \quad (7)$$

$$\frac{dN_d}{dt} = K_d - \mu_d N, \quad (8)$$

Suppose $\frac{N_h(t)}{dt} \geq 0, \frac{N_d(t)}{dt} \geq 0, N_h \geq \frac{K_h}{\mu_h}$ and $N_d \geq \frac{K_d}{\mu_d}$, following which using the differential inequality theorem from [25] yields the following results: $0 \leq N_h \leq \frac{K_h}{\mu_h}$ and $0 \leq N_d \leq \frac{K_d}{\mu_d}$ 7 and 8.

$$\frac{N_h(t)}{dt} \geq K_h - \mu_h N, \quad (9)$$

$$\frac{N_d(t)}{dt} \geq K_d - \mu_d N, \quad (10)$$

Utilizing the integrating factor (IF) approach, solve 9 and 10. Hence, $IF = e^{(\int p(t)dt)}$ and $\frac{dy}{dt} + p(t)y = Q$. After some algebraic adjustments, the region represents a potential solution for the dog population in model system (1).

$$\Omega_d = \left((S_d, I_d, V_d) \in R^3_+, N_d \geq \frac{k_d}{\mu_d} \right), \quad (11)$$

The human population does the same thing. This suggests that the location, 9, may have a resolved human population in model system (1).

$$\Omega_h = \left((S_h, E_h, I_h, V_h, R_h) \in R^5_+, N_h \geq \frac{K_h}{\mu_k} \right), \quad (12)$$

Consequently, the feasible solutions are included in Ω. As per the well accepted comparison theorem on differential inequality in 12, $\Omega = \Omega_h \times \Omega_d$, therefore

$$[N_h \geq N_h(0)]\, e^{-(\mu_h)t} + \frac{K_h}{\mu_h}\left(1 - e^{-(\mu_h)t}\right), \quad (13)$$

$$[N_d \geq N_d(0)]\, e^{-(\mu_d)t} + \frac{K_d}{\mu_d}\left(1 - e^{-(\mu_d)t}\right), \quad (14)$$

Hence, the total dog population size $N_d(t) \to \frac{K_d}{m_d}$ as $t \to \infty$. Similarly the total human population size $N_h(t) \to \frac{K_h}{\mu_h}$ as $t \to \infty$. This mean that the infected state variables (S_h, E_h, I_h, V_h) of the two population tend to zero as time goes to infinity. As a result, as shown in [10], the area Ω is drawing (attracting) every solution in R^8_+, resulting in the model system (1)'s workable solution set.

$$\begin{pmatrix} S_h \\ E_h \\ I_h \\ V_h \\ R_h \\ S_d \\ I_d \\ V_d \end{pmatrix} \in R^8_+ | \begin{pmatrix} S_h \geq 0 \\ E_h \geq 0 \\ I_h \geq 0 \\ V_h \geq 0 \\ R_h \geq 0 \\ S_d \geq 0 \\ I_d \geq 0 \\ V_d \geq 0 \\ N_h \geq \frac{A_h}{m_h} \\ N_d \geq \frac{B_d}{m_d} \end{pmatrix}, \quad (15)$$

Therefore, (1) is both epidemiologically significant and mathematically sound.

Theorem: (Positivity of the Model Solutions) *To demonstrate the positivity of the solutions of the model system* (2) *with initial conditions* (2) *(see* [11]*), we must show that all state variables remain non-negative for all* $t \geq 0$*, given non-negative initial conditions. proof* Each equation in system (2) can be written in the general form

$$\frac{dx}{dt} = f(x), \tag{16}$$

where $x \in \{S_h, E_h, I_h, V_h, R_h, S_d, V_d, I_d\}$. The terms on the right-hand side represent rates of birth, infection, recovery, and death — all of which are non-negative.

If the initial conditions are non-negative, i.e.,

$$S_h(0),\ E_h(0),\ I_h(0),\ V_h(0),$$
$$R_h(0),\ S_d(0),\ V_d(0),\ I_d(0) \geq 0,$$

then the differential equation system can be written as

$$\frac{dx}{dt} = f(x),$$

where $f(x)$ is continuous and satisfies $f(x) \geq -cx$ for some constant $c > 0$. Therefore, the solution remains non-negative for all $t \geq 0$.

For $S_h(t)$:

$$\frac{dS_h}{dt} = K_h + \alpha_3 V_h - (v + \mu_h + \beta_{hd} I_d) S_h. \tag{17}$$

The term K_h is always non-negative, and since $V_h \geq 0$, the expression $\alpha_3 V_h$ is also non-negative. The last term, $-(v + \mu_h + \beta_{hd} I_d) S_h$, is non-positive, ensuring that S_h cannot become negative. By Gronwall's inequality, if $S_h(0) \geq 0$, then $S_h(t) \geq 0$ for all $t \geq 0$.

For $E_h(t)$:

$$\frac{dE_h}{dt} = \beta_{hd} S_h I_d - (\alpha_1 + \alpha_2 + \delta + \mu_h) E_h. \tag{18}$$

Here, $\beta_{hd} S_h I_d \geq 0$, and the term $-(\alpha_1 + \alpha_2 + \delta + \mu_h) E_h$ prevents E_h from becoming negative. Hence, if $E_h(0) \geq 0$, then $E_h(t) \geq 0$ for all $t \geq 0$.

For the remaining compartments $V_h(t), R_h(t), S_d(t), V_d(t), I_d(t)$: Applying the same reasoning to each equation shows that every compartment remains non-negative, provided the initial conditions are non-negative.

Therefore, by the positivity theorem, all state variables

$$S_h,\ E_h,\ I_h,\ V_h,\ R_h,\ S_d,\ V_d,\ I_d$$

remain non-negative for all $t \geq 0$. This establishes that the model is positive.

4 Disease-Free Equilibrium Point (DFE)

If there is no RABV infection in the community, then there are no humans who have received treatment, recovered, or contracted the disease from infected dogs, so that

$$E_h^0 = I_h^0 = I_d^0 = 0.$$

The point F^0 represents the disease-free equilibrium obtained from model equations (2).

$$F^0 = \left(S_h^0, E_h^0, I_h^0, V_h^0, R_h^0, S_d^0, I_d^0, V_d^0\right), \tag{19}$$

$$F^0 = \left(\frac{K_h}{\alpha_3 - (v + \mu_h)},\ 0,\ 0,\ \frac{K_h}{(\alpha_3 - (v + \mu_h))(\alpha_3 + \mu_h)},\right.$$
$$\left. 0,\ \frac{(\mu_d + k_1) K_d}{k(\mu_d + k_1) - K_d},\ 0,\ \frac{K_d}{k(\mu_d + k_1) - K_d}\right), \tag{20}$$

5 Basic Reproduction Number R_0

The basic reproduction number, denoted by R_0, is a fundamental threshold parameter that plays a crucial role in understanding the potential spread and persistence of infectious diseases. It represents the average number of secondary infections produced by a single infected individual in a completely susceptible population. An epidemic occurs when one infected individual transmits the disease to more than one susceptible host, i.e., when $R_0 > 1$. Conversely, if $R_0 < 1$, the infection will eventually die out.

Numerous studies [15, 16] have focused on determining R_0 for various epidemic models. In this study, we compute R_0 for the proposed rabies model using the next-generation matrix approach as described in [16, 20].

5.1 Identification of Infected Compartments

Following the next-generation matrix method, we identify the infected compartments as E_h, I_h, and I_d. The equations governing these compartments are extracted from system (2):

$$\begin{aligned}\frac{dE_h}{dt} &= \beta_{hd} S_h I_d - (\alpha_1 + \alpha_2 + \delta + \mu_h) E_h, \\ \frac{dI_h}{dt} &= \delta E_h - (\mu_h + \mu_1) I_h, \\ \frac{dI_d}{dt} &= \beta_{dd} S_d I_d - \mu_d I_d.\end{aligned} \tag{21}$$

5.2 The Disease-Free Equilibrium (DFE)

At the disease-free equilibrium, we have $E_h^0 = I_h^0 = I_d^0 = 0$. Solving system (2) at steady state yields the DFE:

$$\mathcal{E}^0 = \left(S_h^0, E_h^0, I_h^0, V_h^0, R_h^0, S_d^0, I_d^0, V_d^0\right), \tag{22}$$

where

$$S_h^0 = \frac{K_h(\alpha_3 + \mu_h)}{\mu_h(\alpha_3 + \mu_h) + v\mu_h + \alpha_3 v}, \tag{23}$$

$$V_h^0 = \frac{vK_h}{\mu_h(\alpha_3 + \mu_h) + v\mu_h + \alpha_3 v}, \tag{24}$$

$$S_d^0 = \frac{K_d(\mu_d + k_1)}{k\mu_d}, \tag{25}$$

$$V_d^0 = \frac{K_d}{\mu_d}, \tag{26}$$

$$E_h^0 = I_h^0 = R_h^0 = I_d^0 = 0. \tag{27}$$

5.3 Construction of $\mathcal{F}$ and $\mathcal{V}$ Matrices

The matrix $\mathcal{F}$ represents the rate of new infections appearing in each infected compartment, while $\mathcal{V}$ represents the rate of transfers of individuals into and out of these compartments. At the DFE, we have:

$$F = \begin{pmatrix} 0 & 0 & \beta_{hd} S_h^0 \\ 0 & 0 & 0 \\ 0 & 0 & \beta_{dd} S_d^0 \end{pmatrix}, \qquad V = \begin{pmatrix} A & 0 & 0 \\ -\delta & \mu_h + \mu_1 & 0 \\ 0 & 0 & \mu_d \end{pmatrix}, \tag{28}$$

where $A = \alpha_1 + \alpha_2 + \delta + \mu_h$.

The inverse of V is:

$$V^{-1} = \begin{pmatrix} \frac{1}{A} & 0 & 0 \\ \frac{\delta}{A(\mu_h + \mu_1)} & \frac{1}{\mu_h + \mu_1} & 0 \\ 0 & 0 & \frac{1}{\mu_d} \end{pmatrix}. \tag{29}$$

5.4 The Next-Generation Matrix and R_0

The next-generation matrix is $K = FV^{-1}$:

$$K = \begin{pmatrix} 0 & 0 & \frac{\beta_{hd} S_h^0}{\mu_d} \\ 0 & 0 & 0 \\ 0 & 0 & \frac{\beta_{dd} S_d^0}{\mu_d} \end{pmatrix}. \tag{30}$$

The eigenvalues of K are:

$$\lambda_1 = 0, \quad \lambda_2 = 0, \quad \lambda_3 = \frac{\beta_{dd} S_d^0}{\mu_d}. \tag{31}$$

The basic reproduction number R_0 is the spectral radius of K:

$$R_0 = \rho(K) = \frac{\beta_{dd} S_d^0}{\mu_d}. \tag{32}$$

Substituting $S_d^0 = \frac{K_d(\mu_d + k_1)}{k\mu_d}$ yields the final expression:

$$R_0 = \frac{\beta_{dd} K_d(\mu_d + k_1)}{k\mu_d^2}. \tag{33}$$

5.5 Biological Interpretation of R_0

Equation (33) reveals several important relationships:

- R_0 is directly proportional to β_{dd} (dog-to-dog transmission rate) and K_d (dog birth rate). Increasing either of these parameters will increase the disease's potential to spread.
- R_0 is inversely proportional to k (dog vaccination rate) and μ_d^2 (square of dog mortality rate). This indicates that vaccination campaigns and population management (e.g., culling or sterilization) are effective control strategies.
- The vaccine waning rate k_1 appears in the numerator, meaning that faster loss of immunity in vaccinated dogs increases R_0, highlighting the importance of booster vaccinations.
- The expression is always non-negative and well-defined for all positive parameter values, satisfying biological feasibility.

Figure 2 illustrates the dependence of R_0 on key parameters. As shown in Figure 2(a), R_0 increases with both k_1 and β_{dd}. Figure 2(b) demonstrates the rapid decay of R_0 as μ_d increases, confirming the strong negative impact of dog mortality on disease transmission.

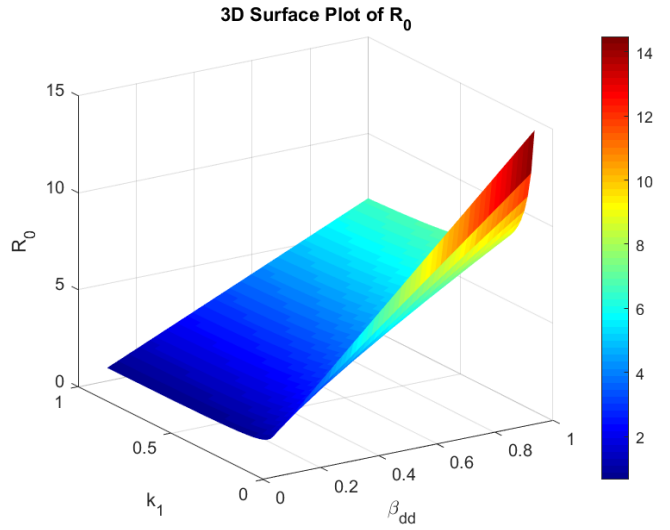

(a) a

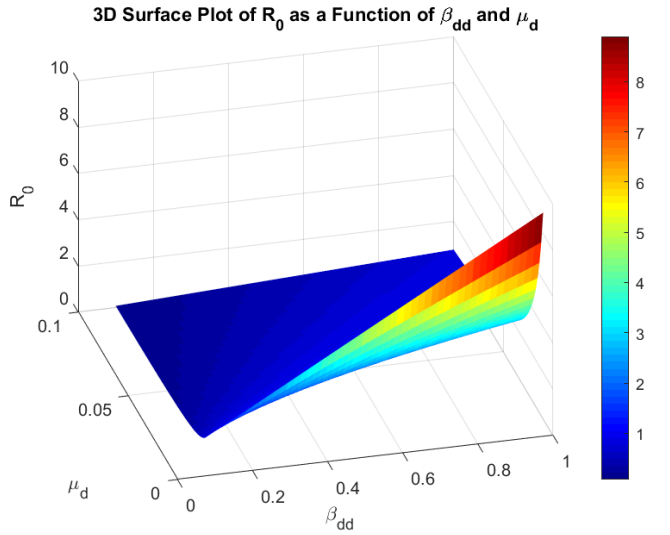

(b) b

Figure 2. Surface plot of R_0 as a function of (a) k_1 and β_{dd}, and (b) as a function of μ_d.

6 Sensitivity Analysis of R_0

Sensitivity analysis of the basic reproduction number R_0 with respect to the model parameters is essential for understanding the dynamics of disease transmission. It helps identify the parameters that have the greatest influence on the prevention and control of the disease. The classical normalized forward sensitivity index of R_0 with respect to a given parameter p is defined as:

$$\Gamma_p^{R_0} = \frac{\partial R_0}{\partial p} \times \frac{p}{R_0}. \tag{34}$$

We compute the sensitivity indices for the parameters that appear in R_0: β_{dd}, K_d, k, μ_d, and k_1.

6.1 Sensitivity Indices

$$\Gamma_{\beta_{dd}}^{R_0} = \frac{\partial R_0}{\partial \beta_{dd}} \cdot \frac{\beta_{dd}}{R_0} = 1, \tag{35}$$

$$\Gamma_{K_d}^{R_0} = \frac{\partial R_0}{\partial K_d} \cdot \frac{K_d}{R_0} = 1, \tag{36}$$

$$\Gamma_{k}^{R_0} = \frac{\partial R_0}{\partial k} \cdot \frac{k}{R_0} = -1, \tag{37}$$

$$\Gamma_{\mu_d}^{R_0} = \frac{\partial R_0}{\partial \mu_d} \cdot \frac{\mu_d}{R_0} = -2 + \frac{\mu_d}{\mu_d + k_1}, \tag{38}$$

$$\Gamma_{k_1}^{R_0} = \frac{\partial R_0}{\partial k_1} \cdot \frac{k_1}{R_0} = \frac{k_1}{\mu_d + k_1}. \tag{39}$$

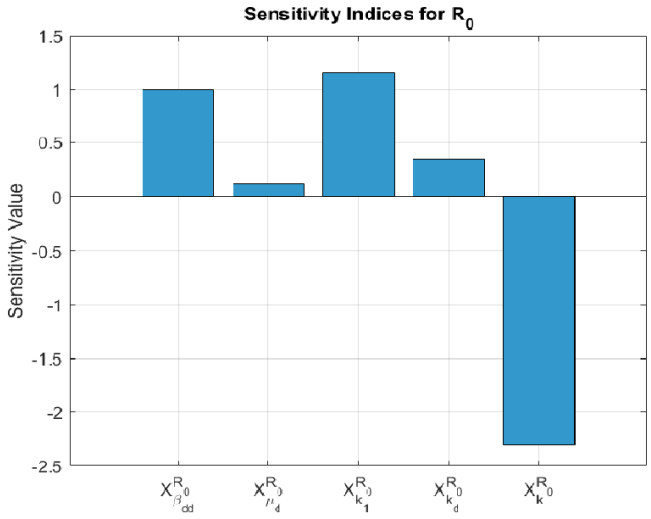

Figure 3. Sensitivity indices of R_0 with respect to key parameters. Positive indices indicate that increasing the parameter increases R_0; negative indices indicate the opposite.

6.2 Interpretation of Sensitivity Results

The sensitivity indices shown in Figure 3 lead to the following conclusions:

- β_{dd} **and** K_d ($\Gamma = +1$): A 1% increase in either the dog-to-dog transmission rate or the dog birth rate results in a 1% increase in R_0. These are the most influential positive parameters.
- k ($\Gamma = -1$): A 1% increase in the dog vaccination rate reduces R_0 by 1%. This confirms that mass dog vaccination is a highly effective control strategy.
- μ_d ($\Gamma = -2 + \frac{\mu_d}{\mu_d + k_1}$): This index lies in the interval $(-2, -1)$. Increasing the natural death rate of dogs (e.g., through population control measures) has a strong negative impact on R_0, reducing disease transmission significantly.

- k_1 ($\Gamma = \frac{k_1}{\mu_d + k_1} \in (0,1)$): The vaccine waning rate has a positive but less-than-proportional effect on R_0. This underscores the need for booster vaccinations to maintain herd immunity.

From a public health perspective, the most effective strategies to control rabies transmission are:

1. Reducing dog-to-dog transmission (β_{dd}) through isolation of infected animals and leash laws,
2. Increasing dog vaccination coverage (k),
3. Implementing population management to increase effective mortality (μ_d), and
4. Maintaining vaccine efficacy through regular booster campaigns (reducing effective k_1).

7 Local Stability of the Disease-Free Equilibrium

The local stability is analyzed via the Jacobian matrix evaluated at the disease-free equilibrium, following standard techniques for nonlinear systems [22]. We now investigate the local stability of the disease-free equilibrium $\mathcal{E}^0$. The Jacobian matrix of system (2) evaluated at $\mathcal{E}^0$ is:

$$J_{\mathcal{E}^0} = \begin{pmatrix} -D_1 & 0 & 0 & \alpha_3 & 0 & 0 & 0 & -\beta_{hd} S_h^0 \\ 0 & -D_2 & 0 & 0 & 0 & 0 & 0 & \beta_{hd} S_h^0 \\ 0 & \delta & -D_3 & 0 & 0 & 0 & 0 & 0 \\ v & \alpha_1 & 0 & -D_4 & 0 & 0 & 0 & 0 \\ 0 & \alpha_2 & 0 & 0 & -D_5 & 0 & 0 & 0 \\ 0 & 0 & 0 & 0 & 0 & -k & k_1 & -\beta_{dd} S_d^0 \\ 0 & 0 & 0 & 0 & 0 & k & -D_7 & 0 \\ 0 & 0 & 0 & 0 & 0 & 0 & 0 & -\mu_d(1 - R_0) \end{pmatrix},$$

where

$$\begin{aligned} D_1 &= v + \mu_h, \\ D_2 &= \alpha_1 + \alpha_2 + \delta + \mu_h, \\ D_3 &= \mu_h + \mu_1, \\ D_4 &= \alpha_3 + \mu_h, \\ D_5 &= \mu_h, \\ D_7 &= \mu_d + k_1. \end{aligned}$$

Theorem 7.1. *The disease-free equilibrium $\mathcal{E}^0$ of system (2) is locally asymptotically stable if $R_0 < 1$, and unstable if $R_0 > 1$.*

Proof. The eigenvalues of $J_{\mathcal{E}^0}$ are:

$$\begin{aligned} \lambda_1 &= -(\mu_h + \mu_1) < 0, \\ \lambda_2 &= -\mu_h < 0, \\ \lambda_3 &= -(\mu_d + k_1) < 0, \\ \lambda_4 &= -(v + \mu_h) < 0, \\ \lambda_5 &= -(\alpha_3 + \mu_h) < 0, \\ \lambda_6 &= -(\alpha_1 + \alpha_2 + \delta + \mu_h) < 0, \\ \lambda_{7,8} &= \text{eigenvalues of } \begin{pmatrix} -k & k_1 \\ 0 & -\mu_d(1 - R_0) \end{pmatrix}. \end{aligned}$$

The eigenvalues $\lambda_{7,8}$ are $-k < 0$ and $-\mu_d(1-R_0)$. Thus, all eigenvalues have negative real parts if and only if $R_0 < 1$. When $R_0 > 1$, the eigenvalue $-\mu_d(1 - R_0)$ becomes positive, leading to instability. □

8 Global Stability of the Disease-Free Equilibrium

To establish the global asymptotic stability of the DFE, we employ the approach proposed by Castillo-Chavez et al. [23]. The system is written in the form:

$$\begin{cases} \dfrac{d\mathbf{X}}{dt} = F(\mathbf{X}, \mathbf{Y}), \\ \dfrac{d\mathbf{Y}}{dt} = G(\mathbf{X}, \mathbf{Y}), \quad G(\mathbf{X}, 0) = 0, \end{cases} \tag{40}$$

where $\mathbf{X} \in \mathbb{R}^5$ represents the uninfected compartments (S_h, V_h, R_h, S_d, V_d), and $\mathbf{Y} \in \mathbb{R}^3$ represents the infected compartments (E_h, I_h, I_d). The DFE is denoted by $\mathcal{E}^0 = (\mathbf{X}^0, 0)$.

The following two conditions must be satisfied for global asymptotic stability:

(H1) For $\dfrac{d\mathbf{X}}{dt} = F(\mathbf{X}, 0)$, the equilibrium $\mathbf{X}^0$ is globally asymptotically stable.

(H2) $G(\mathbf{X}, \mathbf{Y}) = M\mathbf{Y} - \widehat{G}(\mathbf{X}, \mathbf{Y})$, where $\widehat{G}(\mathbf{X}, \mathbf{Y}) \geq 0$ for $(\mathbf{X}, \mathbf{Y}) \in \Omega$, and M is an M-matrix (off-diagonal entries non-negative).

Theorem 8.1. *If $R_0 < 1$ and conditions (H1) and (H2) are satisfied, then the disease-free equilibrium $\mathcal{E}^0$ is globally asymptotically stable in Ω.*

Proof. For the rabies model, we have:

$$F(\mathbf{X}, 0) = \begin{pmatrix} K_h + \alpha_3 V_h - (v + \mu_h) S_h \\ v S_h - (\alpha_3 + \mu_h) V_h \\ -\mu_h R_h \\ K_d + k_1 V_d - k S_d \\ k S_d - (\mu_d + k_1) V_d \end{pmatrix}.$$

It can be shown that $\mathbf{X}^0 = (S_h^0, V_h^0, 0, S_d^0, V_d^0)$ is globally asymptotically stable for this subsystem. Thus condition (H1) holds.

For condition (H2), we compute:

$$M = \begin{pmatrix} -(\alpha_1+\alpha_2+\delta+\mu_h) & 0 & \beta_{hd}S_h^0 \\ \delta & -(\mu_h+\mu_1) & 0 \\ 0 & 0 & \beta_{dd}S_d^0 - \mu_d \end{pmatrix},$$

and

$$\widehat{G}(\mathbf{X}, \mathbf{Y}) = \begin{pmatrix} \beta_{hd}(S_h^0 - S_h)I_d \\ 0 \\ \beta_{dd}(S_d^0 - S_d)I_d \end{pmatrix}.$$

Since $S_h^0 \geq S_h$ and $S_d^0 \geq S_d$ in the feasible region Ω, we have $\widehat{G}(\mathbf{X}, \mathbf{Y}) \geq 0$. Moreover, M has non-negative off-diagonal entries. When $R_0 < 1$, we have $\beta_{dd}S_d^0 - \mu_d < 0$, making M an M-matrix. Hence condition (H2) holds, and the DFE is globally asymptotically stable for $R_0 < 1$. □

9 Endemic Equilibrium

When $R_0 > 1$, the disease persists in the population, and there exists a unique endemic equilibrium $\mathcal{E}^* = (S_h^*, E_h^*, I_h^*, V_h^*, R_h^*, S_d^*, I_d^*, V_d^*)$. Setting the time derivatives of system (2) to zero and solving yields:

$$S_h^* = \frac{K_h + \alpha_3 V_h^*}{v + \mu_h + \beta_{hd} I_d^*}, \tag{41}$$

$$E_h^* = \frac{\beta_{hd} S_h^* I_d^*}{\alpha_1 + \alpha_2 + \delta + \mu_h}, \tag{42}$$

$$I_h^* = \frac{\delta E_h^*}{\mu_h + \mu_1}, \tag{43}$$

$$V_h^* = \frac{\alpha_1 E_h^* + v S_h^*}{\alpha_3 + \mu_h}, \tag{44}$$

$$R_h^* = \frac{\alpha_2 E_h^*}{\mu_h}, \tag{45}$$

$$S_d^* = \frac{K_d + k_1 V_d^*}{k + \beta_{dd} I_d^*}, \tag{46}$$

$$V_d^* = \frac{k S_d^*}{\mu_d + k_1}, \tag{47}$$

$$I_d^* = \frac{k\mu_d(R_0 - 1)}{\beta_{dd}(\mu_d + k_1)}. \tag{48}$$

Note that $I_d^* > 0$ if and only if $R_0 > 1$, confirming the existence of a unique endemic equilibrium when the basic reproduction number exceeds unity.

10 Global Stability of the Endemic Equilibrium

To analyze the global stability of the endemic equilibrium, we construct a Lyapunov function following the approach of Vargas-De-León [21].

Theorem 10.1. *If $R_0 > 1$, the endemic equilibrium $\mathcal{E}^*$ of system (2) is globally asymptotically stable in the interior of Ω.*

Proof. Consider the Lyapunov function:

$$L = \frac{1}{2}\left[(S_h - S_h^*)^2 + (E_h - E_h^*)^2 + (I_h - I_h^*)^2 + (V_h - V_h^*)^2 + (R_h - R_h^*)^2 + (S_d - S_d^*)^2 + (I_d - I_d^*)^2 + (V_d - V_d^*)^2\right].$$

Differentiating L with respect to time and using the fact that at equilibrium the total population satisfies $N_h^* = (K_h - \mu_1 I_h^*)/\mu_h$ and $N_d^* = K_d/\mu_d$, we obtain:

$$\frac{dL}{dt} = (N_h - N_h^*)\frac{dN_h}{dt} + (N_d - N_d^*)\frac{dN_d}{dt}.$$

Since $\frac{dN_h}{dt} = K_h - \mu_h N_h - \mu_1 I_h$ and $\frac{dN_d}{dt} = K_d - \mu_d N_d$, we have:

$$\frac{dL}{dt} = (N_h - N_h^*)(-\mu_h(N_h - N_h^*) - \mu_1(I_h - I_h^*)) + (N_d - N_d^*)(-\mu_d(N_d - N_d^*)).$$

This simplifies to:

$$\frac{dL}{dt} \leq -\mu_h(N_h - N_h^*)^2 - \mu_d(N_d - N_d^*)^2 \leq 0.$$

The equality $\frac{dL}{dt} = 0$ holds only at the endemic equilibrium $\mathcal{E}^*$. By LaSalle's invariance principle, $\mathcal{E}^*$ is globally asymptotically stable when $R_0 > 1$. □

11 Numerical Simulation

The numerical simulations in this study were performed using MATLAB 2016a and the `ODE45` solver, which combines the fourth- and fifth-order Runge–Kutta methods (RK4 and RK5). This solver has proven to be highly accurate for simulating the dynamics of the rabies transmission model. The initial conditions were chosen arbitrarily to illustrate typical model behavior.

Figure 4 shows the temporal dynamics of the rabies population. The results indicate that the proportion of susceptible animals declines rapidly during the

initial years. This reduction is primarily due to disease transmission from infected animals to humans and the depletion of highly susceptible animals. As susceptible animals come into contact with infected humans, their susceptibility decreases while their exposure to the virus increases.

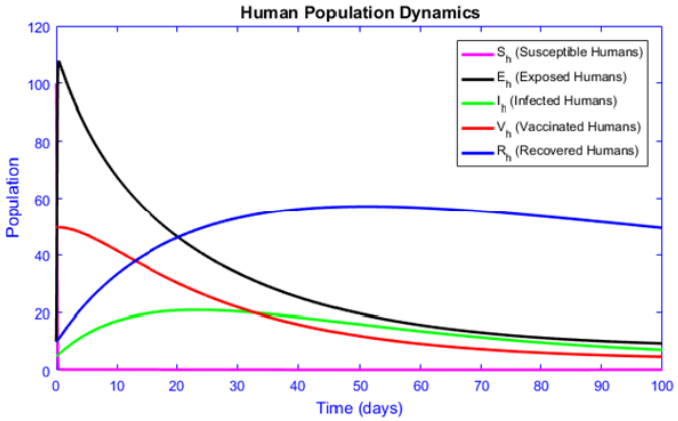

Figure 4. Evolution of Humans Population with time.

The graphical representation of these dynamics provides important insights into the early effects of disease transmission on the rabies population, consistent with the One Health approach [24]. It also emphasizes the critical role of vaccination programs and the importance of controlling infection spread to effectively manage rabies.

If the human-to-dog transmission rate β_{dh} is low (e.g., $\beta_{dh} = 0.001$), the susceptible population declines slowly, indicating a slower rate of disease transmission. In this scenario, the disease spreads less efficiently, and the number of susceptible individuals decreases gradually over time. Conversely, if β_{dh} is high (e.g., $\beta_{dh} = 0.8$), the transmission rate is higher, resulting in a faster spread of the disease. The susceptible population decreases rapidly as more individuals become exposed and infected.

Examining the effect of different β_{dh} values on the exposed population E provides important insights into disease dissemination. Lower β_{dh} values slow the spread of infection, while higher values lead to a rapid increase in exposed individuals, triggering a faster and more extensive epidemic. This underscores the importance of controlling transmission to mitigate the impact of infectious diseases. The findings also emphasize the critical need for interventions that reduce β_{dh}, as illustrated in Figures 5 and 6, which examine the global stability of disease-free equilibrium (DFE). Strategies such as vaccination, social distancing, mask usage, and

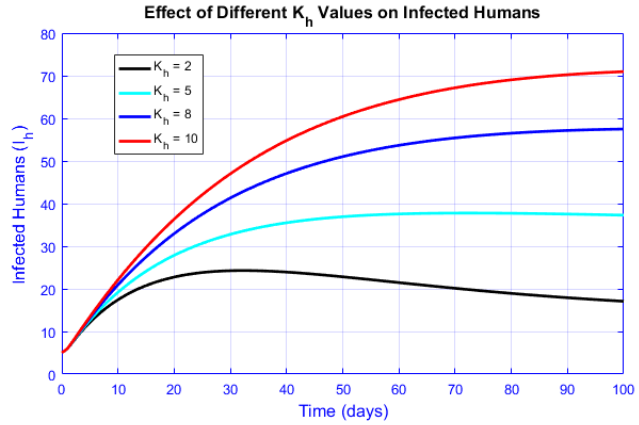

(a)

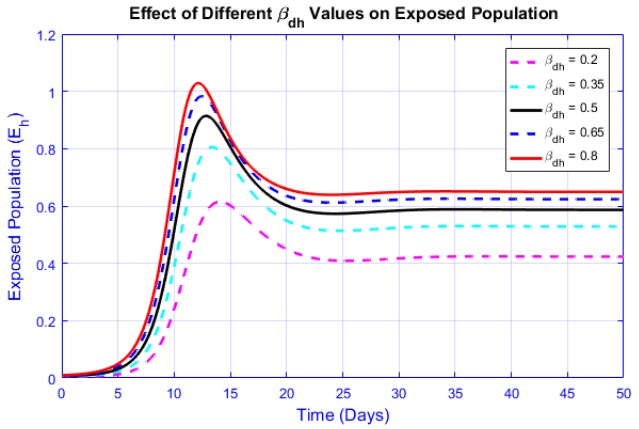

(b)

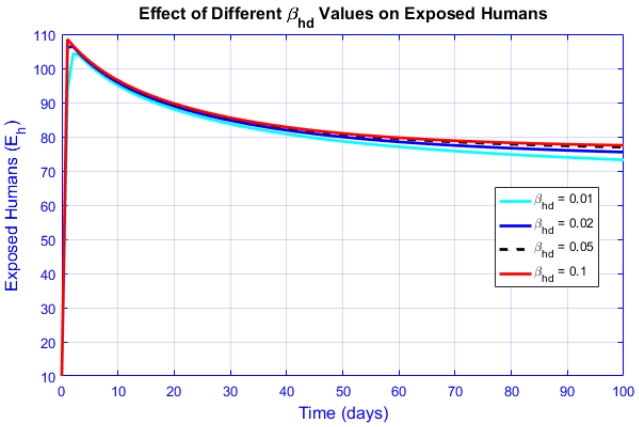

(c)

Figure 5. β_{hd} effect on E.

improved hygiene can effectively lower β_{dh} and reduce disease transmission. Maintaining a lower β_{dh} can prevent a sudden and overwhelming outbreak, reduce the overall disease burden, and facilitate more effective management of healthcare resources.

The practice of immunization significantly reduces the number of vulnerable individuals. Because vaccines are administered promptly, fewer people remain at

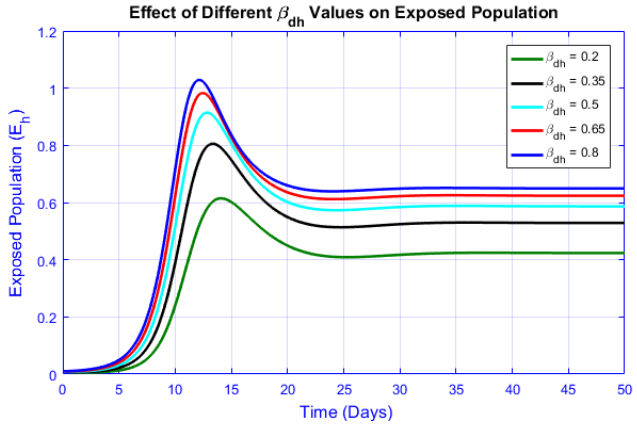

(a)

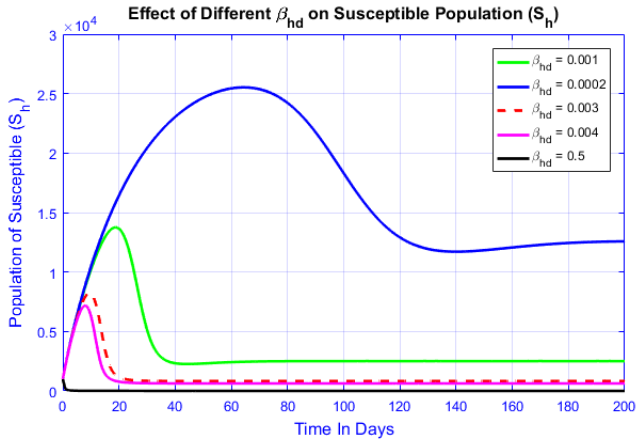

(b)

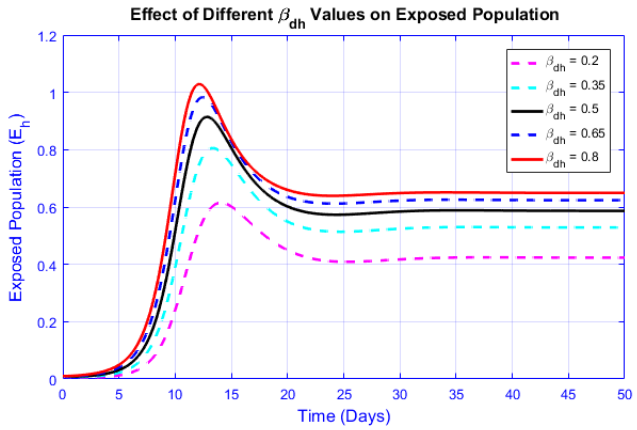

(c)

Figure 6. $\beta_d h$, Different Values E_h, and S_h.

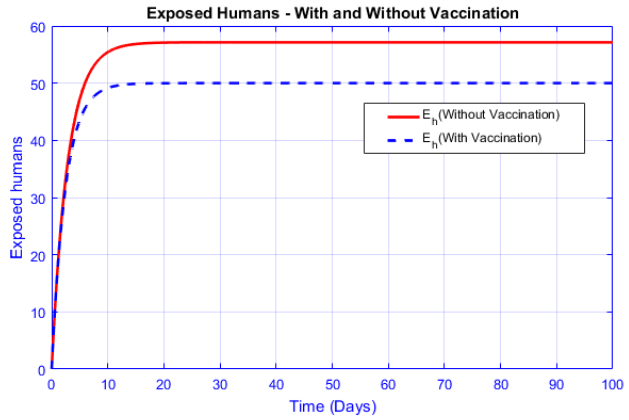

(a)

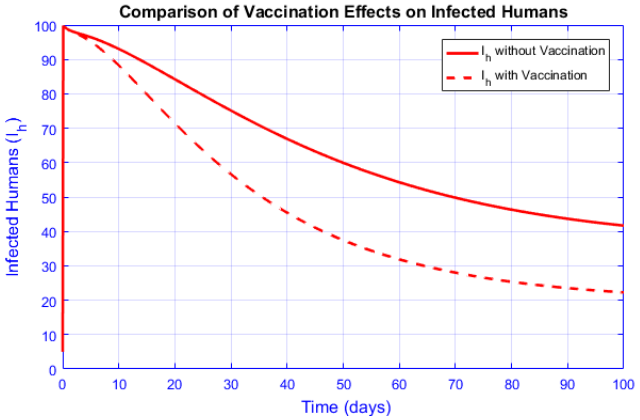

(b)

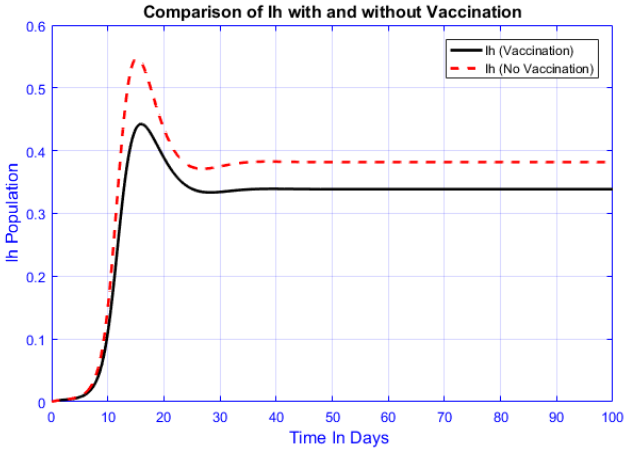

(c)

Figure 7. With Vaccine and with out Vaccine.

risk, leading to a decrease in both exposed and infected populations, as observed in the vaccination scenario. A higher proportion of recovered individuals in the vaccinated case further indicates that immunization plays an essential role in enhancing recovery rates. The vaccinated group clearly demonstrates how immunization limits the transmission of the disease. Overall, Figure 7 these findings show that vaccination effectively reduces the number of at-risk and infected individuals, ultimately resulting in fewer cases and faster recovery within the population.

11.1 Numerical Analysis

This section presents the numerical results of model (2) using the RK4 method and the MATLAB-coded NSFD technique. The parameter values used in the

simulations are collected from [1, 2] and are listed in Table 1. We first develop the numerical schemes for the epidemic model, then illustrate the dynamic behavior of rabies over time t through graphs and simulations. Finally, we discuss and interpret the numerical results.

11.2 RK4 scheme

To give an explicit numerical methodology for the RK4 approach, the following assumptions need to be established [2]. $S(t) \approx S^n \quad E(t) \approx E^n \quad P(t) \approx P^n$ $I(t) \approx I^n \; V(t) \approx V^n \; R(t) \approx R^n$

$$\begin{cases} a_1 &= h[K_h + \alpha_3 V_h^n - (v + \mu_h + \beta_{hd} I_d^n) S_h^n], \\ w_1 &= h[\beta_{hd} S_h^n I_d - (\alpha_1 + \alpha_2 + \delta + \mu_h) E_h^n], \\ m_1 &= h[\delta E_h^n - (\mu_h + \mu_1) I_h^n], \\ n_1 &= h[\alpha_1 E_h^n + v S_h^n - (\alpha_3 + \mu_h) V_h^n], \\ o_1 &= h[\alpha_2 E_h^n - \mu_h R_h^n], \\ q_1 &= [K_d + k_1 V_d^n - (k + \beta_{dd} I_d^n) S_d^n], \\ p_1 &= [k S_d^n - (\mu_d + k_1) V_d^n], \\ v_1 &= [\beta_{dd} S_d^n I_d - \mu_d I_d^n]. \end{cases} \tag{49}$$

$$\tilde{S}_h = S_h^n + \frac{a_1}{2}, \quad \tilde{E}_h = E_h^n + \frac{w_1}{2}, \quad \tilde{I}_h = I_h^n + \frac{m_1}{2},$$
$$\tilde{V}_h = V_h^n + \frac{n_1}{2}, \quad \tilde{R}_h = R_h^n + \frac{o_1}{2},$$
$$\tilde{S}_d = S_d^n + \frac{q_1}{2}, \quad \tilde{V}_d = V_d^n + \frac{p_1}{2}, \quad \tilde{I}_d = I_d^n + \frac{v_1}{2}.$$

$$\begin{aligned} a_2 &= h\big[K_h + \alpha_3 \tilde{V}_h - (v + \mu_h + \beta_{hd} \tilde{I}_d) \tilde{S}_h\big], \\ w_2 &= h\big[\beta_{hd} \tilde{S}_h \tilde{I}_d - (\alpha_1 + \alpha_2 + \delta + \mu_h) \tilde{E}_h\big], \\ m_2 &= h\big[\delta \tilde{E}_h - (\mu_h + \mu_1) \tilde{I}_h\big], \\ n_2 &= h\big[\alpha_1 \tilde{E}_h + v \tilde{S}_h - (\alpha_3 + \mu_h) \tilde{V}_h\big], \\ o_2 &= h\big[\alpha_2 \tilde{E}_h - \mu_h \tilde{R}_h\big], \\ q_2 &= h\big[K_d + k_1 \tilde{V}_d - (k + \beta_{dd} \tilde{I}_d) \tilde{S}_d\big], \\ p_2 &= h\big[k \tilde{S}_d - (\mu_d + k_1) \tilde{V}_d\big], \\ v_2 &= h\big[\beta_{dd} \tilde{S}_d \tilde{I}_d - \mu_d \tilde{I}_d\big]. \end{aligned}$$

$$\begin{aligned} a_3 &= h\Big[K_h + \alpha_3\Big(V_h^n + \frac{n_2}{2}\Big) - \Big(v + \mu_h + \beta_{hd}\Big(I_d^n + \frac{v_2}{2}\Big)\Big)\Big(S_h^n + \frac{a_2}{2}\Big)\Big], \\ w_3 &= h\Big[\beta_{hd}\Big(S_h^n + \frac{a_2}{2}\Big)\Big(I_d^n + \frac{v_2}{2}\Big) - (\alpha_1 + \alpha_2 + \delta + \mu_h)\Big(E_h^n + \frac{w_2}{2}\Big)\Big], \\ m_3 &= h\Big[\delta\Big(E_h^n + \frac{w_2}{2}\Big) - (\mu_h + \mu_1)\Big(I_h^n + \frac{m_2}{2}\Big)\Big], \\ n_3 &= h\Big[\alpha_1\Big(E_h^n + \frac{w_2}{2}\Big) + v\Big(S_h^n + \frac{a_2}{2}\Big) - (\alpha_3 + \mu_h)\Big(V_h^n + \frac{n_2}{2}\Big)\Big], \\ o_3 &= h\Big[\alpha_2\Big(E_h^n + \frac{w_2}{2}\Big) - \mu_h\Big(R_h^n + \frac{o_2}{2}\Big)\Big], \\ q_3 &= h\Big[K_d + k_1\Big(V_d^n + \frac{p_2}{2}\Big) - \Big(k + \beta_{dd}\Big(I_d^n + \frac{v_2}{2}\Big)\Big)\Big(S_d^n + \frac{q_2}{2}\Big)\Big], \\ p_3 &= h\Big[k\Big(S_d^n + \frac{q_2}{2}\Big) - (\mu_d + k_1)\Big(V_d^n + \frac{p_2}{2}\Big)\Big], \\ v_3 &= h\Big[\beta_{dd}\Big(S_d^n + \frac{q_2}{2}\Big)\Big(I_d^n + \frac{v_2}{2}\Big) - \mu_d\Big(I_d^n + \frac{v_2}{2}\Big)\Big]. \end{aligned}$$

$$\begin{aligned} a_4 &= h\Big[K_h + \alpha_3(V_h^n + n_3) - \big(v + \mu_h + \beta_{hd}(I_d^n + v_3)\big)(S_h^n + a_3)\Big], \\ w_4 &= h\Big[\beta_{hd}(S_h^n + a_3)(I_d^n + v_3) - (\alpha_1 + \alpha_2 + \delta + \mu_h)(E_h^n + w_3)\Big], \\ m_4 &= h\Big[\delta(E_h^n + w_3) - (\mu_h + \mu_1)(I_h^n + m_3)\Big], \\ n_4 &= h\Big[\alpha_1(E_h^n + w_3) + v(S_h^n + a_3) - (\alpha_3 + \mu_h)(V_h^n + n_3)\Big], \\ o_4 &= h\Big[\alpha_2(E_h^n + w_3) - \mu_h(R_h^n + o_3)\Big], \\ q_4 &= h\Big[K_d + k_1(V_d^n + p_3) - \big(k + \beta_{dd}(I_d^n + v_3)\big)(S_d^n + q_3)\Big], \\ p_4 &= h\Big[k(S_d^n + q_3) - (\mu_d + k_1)(V_d^n + p_3)\Big], \\ v_4 &= h\Big[\beta_{dd}(S_d^n + q_3)(I_d^n + v_3) - \mu_d(I_d^n + v_3)\Big]. \end{aligned}$$

$$\begin{aligned} a_7 &= h\Big[K_h + \alpha_3(V_h^n + n_7) - \big(v + \mu_h + \beta_{hd}(I_d^n + v_7)\big)(S_h^n + a_7)\Big], \\ w_7 &= h\Big[\beta_{hd}(S_h^n + a_7)(I_d^n + v_7) - (\alpha_1 + \alpha_2 + \delta + \mu_h)(E_h^n + w_7)\Big], \\ m_7 &= h\Big[\delta(E_h^n + w_7) - (\mu_h + \mu_1)(I_h^n + m_7)\Big], \\ n_8 &= h\Big[\alpha_1(E_h^n + w_7) + v(S_h^n + a_7) - (\alpha_3 + \mu_h)(V_h^n + n_7)\Big], \\ o_8 &= h\Big[\alpha_2(E_h^n + w_7) - \mu_h(R_h^n + o_7)\Big], \\ q_8 &= h\Big[K_d + k_1(V_d^n + p_7) - \big(k + \beta_{dd}(I_d^n + v_7)\big)(S_d^n + q_7)\Big], \\ p_8 &= h\Big[k(S_d^n + q_7) - (\mu_d + k_1)(V_d^n + p_7)\Big], \\ v_8 &= h\Big[\beta_{dd}(S_d^n + q_7)(I_d^n + v_7) - \mu_d(I_d^n + v_7)\Big]. \end{aligned}$$

$$S_h^{n+1} = S_h^n + \frac{1}{16}\Big(k_1 + 2k_2 + 2k_3 + 2k_4 + 2k_5 + 2k_6 + 2k_7 + k_8\Big) \tag{50}$$

$$E_h^{n+1} = E_h^n + \frac{1}{16}\Big(w_1 + 2w_2 + 2w_3 + 2w_4 + 2w_5 + 2w_6 + 2w_7 + w_8\Big) \tag{51}$$

$$I_h^{n+1} = I_h^n + \frac{1}{16}\Big(m_1 + 2m_2 + 2m_3 + 2m_4 + 2m_5 + 2m_6 + 2m_7 + m_8\Big), \tag{52}$$

$$V_h^{n+1} = V_h^n + \frac{1}{16}\Big(n_1 + 2n_2 + 2n_3 + 2n_4 + 2n_5 + 2n_6 + 2n_7 + n_8\Big), \tag{53}$$

$$R_h^{n+1} = R_h^n + \frac{1}{16}\Big(o_1 + 2o_2 + 2o_3 + 2o_4 + 2o_5 + 2o_6 + 2o_7 + o_8\Big), \tag{54}$$

$$S_d^{n+1} = S_d^n + \frac{1}{16}\Big(p_1 + 2p_2 + 2p_3 + 2p_4 + 2p_5 + 2p_6 + 2p_7 + p_8\Big), \tag{55}$$

$$I_d^{n+1} = I_d^n + \frac{1}{16}\Big(q_1 + 2q_2 + 2q_3 + 2q_4 + 2q_5 + 2q_6 + 2q_7 + q_8\Big), \tag{56}$$

$$V_d^{n+1} = V_d^n + \frac{1}{16}\Big(v_1 + 2v_2 + 2v_3 + 2v_4 + 2v_5 + 2v_6 + 2v_7 + v_8\Big). \tag{57}$$

11.3 NSFD scheme

The non-standard finite difference (NSFD) technique developed in [18] serves as the foundation for the reliable numerical method used in this study. The NSFD method preserves important qualitative properties such as positivity and boundedness, consistent with findings in nonstandard computational analyses of rabies models [26]. This method can be applied in various ways to examine practical, real-world problems in mathematics and engineering. For examples of the NSFD approach applied to different areas of applied mathematics, see [19]. Based on the first equation of model (1), the following assumptions are made to present a clear numerical technique for applying the NSFD methodology to equations (1) through (8) of model (1).

$$\begin{cases} \frac{S_h}{dt} = \frac{S_h^{n+1}-S_h}{h}, S_h(t) \approx S_h^{n+1}, I_h(t)S_h(t) = I_h^n S_h^{n+1} \\ \frac{E_h}{dt} = \frac{E_h^{n+1}-E_h}{h}, E_h(t) \approx E_h^{n+1}, I_h(t)S_h(t) = I_h^n S_h^{n+1} \\ \frac{I_h}{dt} = \frac{I_h^{n+1}-I_h}{h}, I_h(t) \approx I_h^{n+1}, \\ \frac{V_h}{dt} = \frac{V_h^{n+1}-V_h}{h}, V_h(t) \approx V_h^{n+1}, E_h(t) = E_h^n \\ \frac{R_h}{dt} = \frac{R_h^{n+1}-R_h}{h}, R_h(t) \approx R_h^{n+1}, \\ \frac{S_d}{dt} = \frac{S_d^{n+1}-S_d}{h}, S_d(t) \approx S_d^{n+1}, I_d(t)S_d(t) = I_d^n S_d^{n+1}, \\ \frac{I_d}{dt} = \frac{I_d^{n+1}-I_d}{h}, I_d(t) \approx E_d^{n+1}, E_d(t) = E_d^n, \\ \frac{V_d}{dt} = \frac{V_d^{n+1}-V_d}{h}, V_h(t) \approx V_d^{n+1}, \end{cases} \tag{58}$$

Using the aforementioned presumption, the model (1)'s eight equations become, Therefore,

$$S_h^{n+1} = \frac{S_h^n + h(K_h + \alpha_3 V_h^n)}{1 + h(\mu_h + \beta_{dh} I_d^n)} \tag{59}$$

$$E_h^{n+1} = \frac{E_h^n + h(\beta_{dh} I_h^n S_h^n)}{1 + h(\alpha_1 + \alpha_2 + \delta + \mu_h)} \tag{60}$$

$$I_h^{n+1} = \frac{I_h^n + h\delta E_h^n}{1 + h(\mu_h + \mu_1)} \tag{61}$$

$$V_h^{n+1} = \frac{V_h^n + h(vS_h^n + \alpha_1 V_h^n)}{1 + (\alpha_3 + \mu_h)} \tag{62}$$

$$R_h^{n+1} = \frac{R_h^n + \alpha_2 E_h^n}{1 + h(\mu_h)}, \tag{63}$$

$$S_d^{n+1} = \frac{S_d^n + h(K_d + k_1 V_d^n)}{1 + h(k + \beta_{dd} I_d^n)} \tag{64}$$

$$V_d^{n+1} = \frac{V_d^n + h(kS_d^n)}{1 + h(\mu_d + k_1)} \tag{65}$$

Theorem: *The equilibrium points (E_0 and E_1, respectively) of the continuous model (1) are preserved by the discrete schemes 59 and 65. In other words, the only fixed points in schemes 59 and 65 correspond either to the disease-free equilibrium or to the endemic equilibrium of the continuous model (1). Moreover, the equilibrium points and the fixed points of the NSFD scheme share the same stability properties.* Figure 8 compares the solutions obtained by the classical RK4 method and the NSFD scheme for the key compartments (S_h, E_h, I_h, R_h). It is evident that both methods produce qualitatively similar trajectories in the short term, but the NSFD scheme better preserves the positivity and boundedness of the solutions, especially for larger time-step sizes.

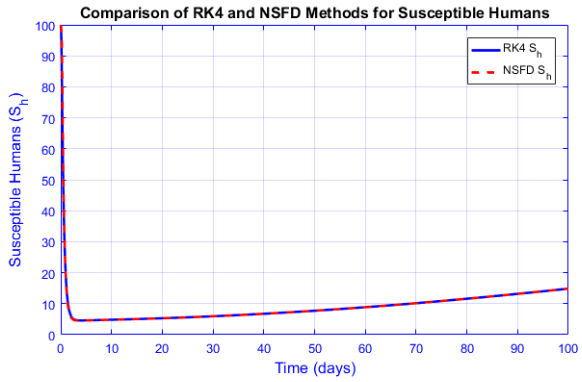

(a)

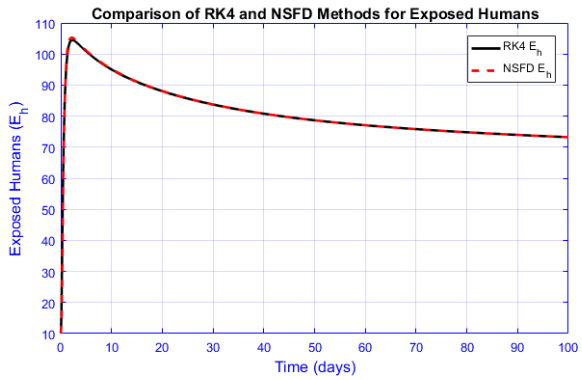

(b)

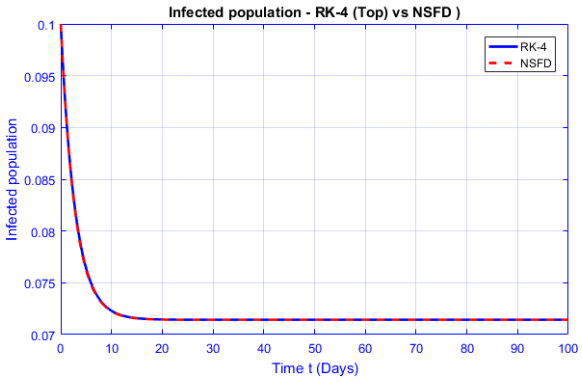

(c)

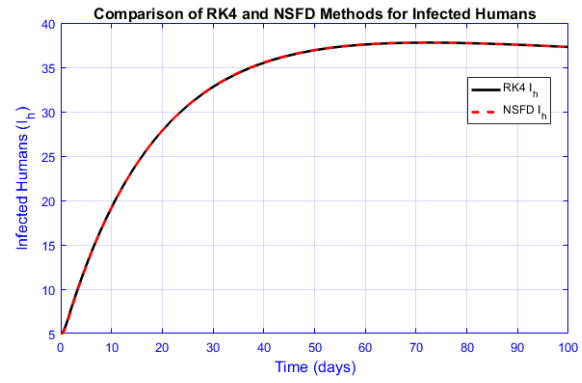

(d)

Figure 8. Rk-4 and NSFD Method.

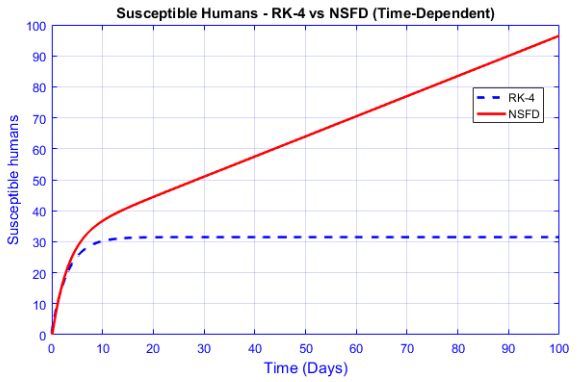

(a)

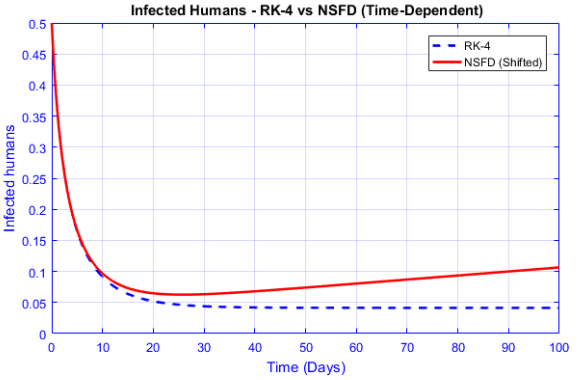

(b)

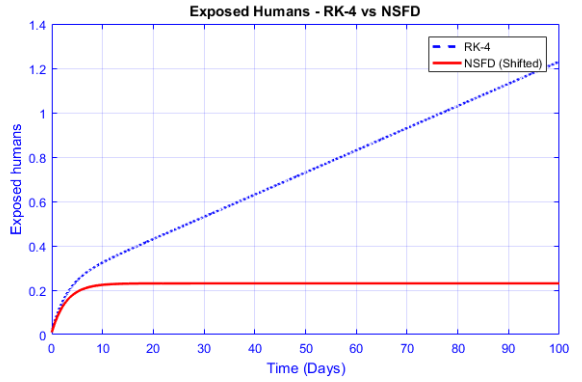

(c)

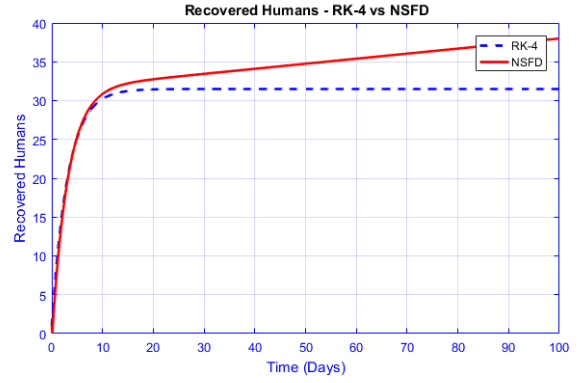

(d)

Figure 9. RK-4 vs NSFD (Time-Dependent).

12 Discussion

Both the Nonstandard Finite Difference (NSFD) scheme and the fourth-order Runge Kutta (RK4) method demonstrate different behaviors when simulating the dynamics of the susceptible S_h, infected I_h, recovered R_h, and exposed populations. The RK4 method, shown by the dashed blue line in Figure 9, is widely recognized for its high accuracy and numerical stability. Its simulation of the exposed population over time clearly reflects the progression and transmission dynamics of the disease. In contrast, the NSFD method, represented by the solid red line, is designed to preserve important qualitative properties of the model, such as stability, boundedness, and non-negativity of solutions. These properties are especially important in epidemiological modeling, where negative population values are not meaningful. Although RK4 generally provides more accurate results due to its fourth-order convergence, both methods may exhibit similar oscillatory trends in certain compartments, including the exposed class. The performance of the NSFD scheme can vary depending on the structure of the model and the chosen parameter values. In many simulations, the RK4 curves appear smoother and more closely aligned with expected theoretical trends. However, NSFD offers advantages when it is necessary to maintain the inherent structural characteristics of the system. Therefore, the choice between RK4 and NSFD should depend on the objectives of the study and the nature of the mathematical model. For simulations that prioritize numerical accuracy and precise prediction, RK4 is often preferred. On the other hand, when preserving qualitative features such as positivity and dynamical consistency is essential, the NSFD method provides a reliable alternative.

This research observes that the results of both numerical techniques are similar when investigating the susceptible population dynamics that are established by the Runge-Kutta 4th order (RK4) and Nonstandard Finite Difference (NSFD) methods. These methods effectively track a prevalence over time in the population of interest. Moreover, while comparing Runge-Kutta 4th order (RK4) and Nonstandard Finite Difference (NSFD) methods for analyzing the dynamics of the infected population, the analysis shows that both methods provide understanding of how the infected population behaves over time.

The dashed blue line represents the RK4 solution, which is highly reliable for approximating the dynamical behavior due to its accuracy in solving ODEs. To enhance structural precision, the NSFD method, depicted by the solid red line, incorporates a time-dependent linear perturbation while the core mechanism remains invariant. In conclusion, although both methods provide insight into the dynamics of the sensitive population, the RK4 approach is often preferred because it is accurate and robust, especially when higher precision is required. However, the NSFD technique remains attractive for certain studies depending on specific requirements, as it possesses distinctive properties that help preserve the stability of the model and ensure non-negativity.

13 Conclusion

In this study, we developed and analyzed an extended mathematical model for rabies transmission that incorporates the Exposed (E_h) and Recovered (R_h) compartments in the human population, alongside the standard compartments for both humans and dogs. The inclusion of these additional classes allows for a more realistic representation of disease progression, treatment response, and transmission dynamics. We analyzed the model for positivity and boundedness of solutions, computed the basic reproduction number (R_0), performed sensitivity analysis, and investigated the global stability of endemic equilibrium points. Our numerical simulations, conducted using both the fourth-order Runge-Kutta (RK4) method and the Nonstandard Finite Difference (NSFD) method, demonstrate that both approaches can effectively capture the dynamics of rabies transmission. While RK4 provides high accuracy in predicting population trends, NSFD preserves important qualitative properties such as stability and non-negativity, which are essential in epidemiological modeling. The results highlight the critical role of vaccination and timely interventions in reducing the susceptible and exposed populations, increasing recovery rates, and ultimately controlling rabies outbreaks. This work underscores the importance of selecting appropriate numerical methods and control strategies based on the goals of the study and the characteristics of the modeled system. The findings can inform public health planning and provide a framework for future studies on rabies control.

Data Availability Statement

Data will be made available on request.

Funding

This work was supported without any funding.

Conflicts of Interest

The authors declare no conflicts of interest.

AI Use Statement

The authors declare that no generative AI was used in the preparation of this manuscript.

Ethical Approval and Consent to Participate

Not applicable.

References

[1] Hampson, K., Coudeville, L., Lembo, T., Sambo, M., Kieffer, A., Attlan, M., ... & Global Alliance for Rabies Control Partners for Rabies Prevention. (2015). Estimating the global burden of endemic canine rabies. *PLoS neglected tropical diseases, 9*(4), e0003709. [CrossRef]

[2] Layan, M., Dellicour, S., Baele, G., Cauchemez, S., & Bourhy, H. (2021). Mathematical modelling and phylodynamics for the study of dog rabies dynamics and control: A scoping review. *PLOS Neglected Tropical Diseases, 15*(5), e0009449. [CrossRef]

[3] Younas, H., Ahmad, I., Ali, N., Haq, I. U., Albalwi, M. D., Muhammad, S., & Shuaib, M. (2024). Modeling rabies dynamics: the impact of vaccination and infectious immigrants on public health. Contemp. *Math, 5*(3), 3255. [CrossRef]

[4] Ruan, S. (2017). Spatiotemporal epidemic models for rabies among animals. *Infectious disease modelling, 2*(3), 277-287. [CrossRef]

[5] Zinsstag, J., Dürr, S., Penny, M. A., Mindekem, R., Roth, F., Gonzalez, S. M., ... & Hattendorf, J. (2009). Transmission dynamics and economics of rabies control in dogs and humans in an African city. *Proceedings of the National Academy of Sciences, 106*(35), 14996-15001. [CrossRef]

[6] Eze, O. C., Mbah, G. E., Nnaji, D. U., & Onyiaji, N. E. (2020). Mathematical modelling of transmission dynamics of rabies virus. *International Journal of Mathematics Trends and Technology-IJMTT, 66*. [CrossRef]

[7] Jehangir, H., Ali, N., Ahmad, I., Younas, H., Ahmad, Z., & El-Agamy, R. F. (2024). Global Dynamics and Numerical Simulation of a Vaccinated Mathematical Model for Rabies Disease. *Global Journal of Sciences, 1*(1), 14-27. [CrossRef]

[8] Hemachudha, T., Ugolini, G., Wacharapluesadee, S., Sungkarat, W., Shuangshoti, S., & Laothamatas, J. (2013). Human rabies: neuropathogenesis, diagnosis, and management. *The Lancet Neurology, 12*(5), 498-513. [CrossRef]

[9] Fisher, C. R., Streicker, D. G., & Schnell, M. J. (2018). The spread and evolution of rabies virus: conquering new frontiers. *Nature Reviews Microbiology, 16*(4), 241-255. [CrossRef]

[10] Demirci, E. (2014). A new mathematical approach for Rabies endemy. *Appl. Math. Sci, 8*(2), 59-67. [CrossRef]

[11] Asano, E., Gross, L. J., Lenhart, S., & Real, L. A. (2008). Optimal control of vaccine distribution in a rabies metapopulation model. *Mathematical Biosciences and Engineering, 5*(2), 219–238. [CrossRef]

[12] Sinan, M., & Khan, A. (2020). Analytic approximate solution of rabies transmission dynamics using homotopy perturbation method. *Matrix Science Mathematics, 4*(1), 01–05. [CrossRef]

[13] Clayton, T., Duke-Sylvester, S., Gross, L. J., Lenhart, S., & Real, L. A. (2010). Optimal control of a rabies epidemic model with a birth pulse. *Journal of Biological Dynamics, 4*(1), 43–58. [CrossRef]

[14] Pantha, B., Joshi, H., & Vaidya, N. (2020). Controlling rabies epidemics in Nepal with limited resources: optimal control theory approach. *Mathematics in Applied Sciences and Engineering, 1*(4), 355-372. [CrossRef]

[15] Diekmann, O., Heesterbeek, J. A. P., & Metz, J. A. (1990). On the definition and the computation of the basic reproduction ratio R_o in models for infectious diseases in heterogeneous populations. *Journal of Mathematical Biology, 28*(4), 365-382. [CrossRef]

[16] van den Driessche, P., & Watmough, J. (2002). Reproduction numbers and sub-threshold endemic equilibria for compartmental models of disease transmission. *Mathematical Biosciences, 180*(1-2), 29-48. [CrossRef]

[17] Ullah, H., Ali, A., & Younas, H. (2025). Modeling the impact of vaccination and post-treatment on rabies transmission. *Journal of Numerical Simulations in Physics and Mathematics, 1*(2), 84–97. [CrossRef]

[18] Mickens, R. E. (1994). *Nonstandard Finite Difference Models of Differential Equations*. World Scientific. [CrossRef]

[19] Otoo, D., Donkoh, E. K., Chuaya, R. G., Mensah, K., Sebil, C., Danquah, B. A., & Adusei, H. (2025). Modeling and Analysis of the Dynamics of Rabies using Nonstandard Finite Difference Approach with Optimal Control. *Appl. Math, 19*(5), 1013-1026. [CrossRef]

[20] Anderson, R. M., & May, R. M. (1991). *Infectious Diseases of Humans: Dynamics and Control*. Oxford University Press. [CrossRef]

[21] Vargas-De-León, C. (2009). Constructions of Lyapunov functions for classic SIS, SIR and SIRS epidemic models with variable population size. *Foro-Red-Mat: Revista electrónica de contenido matemático,*

26(5), 1-12.

[22] Khalil, H. K., & Grizzle, J. W. (2002). *Nonlinear systems* (Vol. 3, p. 126). Upper Saddle River, NJ: Prentice hall.

[23] Castillo-Chavez, C., Feng, Z., & Huang, W. (2002). On the computation of R_0 and its role on global stability. In *Mathematical Approaches for Emerging and Reemerging Infectious Diseases: An Introduction* (Vol. 125, pp. 229-250). IMA Volumes in Mathematics and its Applications, Springer. [CrossRef]

[24] Zinsstag, J., Schelling, E., Waltner-Toews, D., & Tanner, M. (2011). From "one medicine" to "one health" and systemic approaches to health and well-being. *Preventive veterinary medicine, 101*(3-4), 148-156. [CrossRef]

[25] Ullah, S., Ahmad, I., Idrees, M., Islam, S., & Ali, I. (2026). Analysis of tuberculosis transmission dynamics with environmental and reinfection factors: a mathematical approach. *Journal of Applied Mathematics and Computing, 72*(2), 86. [CrossRef]

[26] F. Alfwzan, W., Raza, A., Ahmed, N., Elsonbaty, A., Rafiq, M., & Adel, W. (2024). Nonstandard computational and bifurcation analysis of the rabies epidemic model. *Journal of Mathematics, 2024*(1), 3909089. [CrossRef]